Takeda S, Igarashi T, Mori H	Crystal structure of RVV-X: An example of evolutionary gain of specificity by ADAM proteinases	FEBS Lett	581 (30)	5859-5864	2007
Beppu K, Kaneko Y, Kadokawa J-i, Mori H, Nishikawa T	Synthesis of Sugar-Polysiloxane Hybrids Having Rigid Main-Chains and Formation of their Nano Aggregates	Polymer Journal	39 (10)	1065-1070	2007
Fukuyama N, Jujo S, Ito I, Shizuma T, Myojin K, Ishiwata K, Nagano M, Nakazawa H, Mori H	Kurozu moromimatsu inhibits tumor growth of Lovo cells in a mouse model in vivo	Nutrition	23 (1)	81-86	2007
Fukuyama N, Tanaka E, Tabata Y, Fujikura H, Hagihara M, Sakamoto H, Ando K, Nakazawa H, Mori H	Intravenous injection of phagocytes transfected ex vivo with FGF4 DNA/biodegradable gelatin complex promotes angiogenesis in a rat myocardial ischemia/reperfusion injury model	Basic Res Cardiol	102 (3)	209-216	2007
Igarashi T, Araki S, Mori H, Takeda S	Crystal structures of catrocollastatin/VAP2B reveal a dynamic, modular architecture of ADAM/adamalysin/reprolys in family proteins	FEBS Lett	581 (13)	2416-2422	2007
Kawada T, Kitagawa H, Yamazaki T, Akiyama T, Kamiya A, Uemura K, Mori H, Sugimachi M	Hypothermia reduces ischemia- and stimulation-induced myocardial interstitial norepinephrine and acetylcholine releases	J Appl Physiol	102 (2)	622-627	2007
Kawada T, Yamazaki T, Akiyama T, Li M, Zheng C, Shishido T, Mori H, Sugimachi M	Angiotensin II attenuates myocardial interstitial acetylcholine release in response to vagal stimulation	Am J Physiol Heart Circ Physiol	293 (4)	H2516-2522	2007
Kawada T, Yamazaki T, Akiyama T, Shishido T, Shimizu S, Mizuno M, Mori H, Sugimachi M	Regional difference in ischaemia-induced myocardial interstitial noradrenaline and acetylcholine releases	Auton Neurosci	137 (1-2)	44-50	2007

Kuroko Y, Yamazaki T, Tokunaga N, Akiyama T, Kitagawa H, Ishino K, Sano S, Mori H	Cardiac epinephrine synthesis and ischemia-induced myocardial epinephrine release	Cardiovasc Res	74 (3)	438-444	2007
Myojin K, Taguchi A, Umetani K, Fukushima K, Nishiura N, Matsuyama T, Kimura H, Stern DM, Imai Y, Mori H	Visualization of intracerebral arteries by synchrotron radiation microangiography	AJNR Am J Neuroradiol	28 (5)	953-957	2007
Sagae M, Sato E, Tanaka E, Mori H, Kawai T, Inoue T, Ogawa A, Sato S, Takayama K, Onagawa J, Ido H	Intense clean characteristic flash x-ray irradiation from an evaporating molybdenum diode	Opt. Eng.	46 (026502)	1-7	2007
Sato E, Germer R, Obara H, Tanaka E, Mori H, Kawai T, Inoue T, Ogawa A, Izumisawa M, Ichimaru T, Takahashi K, Sato S, Takayama K	Novel monochromatic x-ray generators and their applications to high-speed radiography (6279)	SPIE	627906	1-12	2007
Sato E, Sagae M, Tanaka E, Mori H, Kawai T, Inoue T, Ogawa A, Sato S, Ichimaru T, Takayama K	High-sensitive radiography system utilizing a pulse x-ray generator and a night-vision CCD camera (MLX) (Proc.)	SPIE	6279 (627941)	1-6	2007
Sato E, Tanaka E, Mori H, Kawakami H, Kawai T, Inoue T, Ogawa A, Izumisawa M, Takahashi K, Sato S, Takayama K, Onagawa J	K-edge magnification digital angiography using a 100-μm-focus tungsten tube	Opt. Eng.	46 (026503)	1-6	2007
Sukmawan R, Yada T, Toyota E, Neishi Y, Kume T, Shinozaki Y, Mori H, Ogasawara Y, Kajiya F, Yoshida K	Edaravone preserves coronary microvascular endothelial function after ischemia/reperfusion on the beating canine heart in vivo	J Pharmacol Sci	104 (4)	341-348	2007
Yada T, Shimokawa H, Hiramatsu O, Shinozaki Y, Mori H, Goto M, Ogasawara Y, Kajiya F	Important role of endogenous hydrogen peroxide in pacing-induced metabolic coronary vasodilation in dogs in vivo	J Am Coll Cardiol	50 (13)	1272-1278	2007

Yamazaki T, Akiyama T, Kitagawa H, Komaki F, Mori H, Kawada T, Sunagawa K, Sugimachi M	Characterization of ouabain-induced noradrenaline and acetylcholine release from in situ cardiac autonomic nerve endings	Acta Physiol (Oxf)	191 (4)	275-284	2007
Obata H, Sakai Y, Ohnishi S, Takeshita S, Mori H, Kodama M, Kangawa K, Aizawa Y, Nagaya N	Single Injection of a Sustained-release Prostacyclin Analog Improves Pulmonary Hypertension in Rats	Am J Respir Crit Care Med	177(2)	195-201	2008
Yada T, Shimokawa H, Morikawa K, Takaki A, Shinozaki Y, Mori H, Goto M, Ogasawara Y, Kajiya F	Role of Cu, Zn-SOD in the Synthesis of Endogenous Vasodilator Hydrogen Peroxide during Reactive Hyperemia in Mouse Mesenteric Microcirculation in Vivo	Am J Physiol Heart Circ Physiol	294(1)	H441-448	2008
武田壮一	ADAMファミリータンパク質のドメイン構造	生化学	79 (11)	1051-1055	2007
武田壮一	蛇毒メタロプロテアーゼの結晶構造とADAMファミリーの基質認識機構	日本結晶学会誌	49	192-197	2007
Nakaoka Y, Nishida K, Narimatsu M, Kamiya A, Minami T, Sawa H, Okawa K, Fujio Y, Koyama T, Maeda M, Sone M, Yamasaki S, Arai Y, Koh GY, Kodama T, Hirota H, Otsu K, Hirano T, Mochizuki N	Gab family proteins are essential for postnatal maintenance of cardiac function via neuregulin-1/ErbB signaling	J Clin Invest	117(7)	1771-1781	2007
Takaya A, Kamio T, Masuda M, Mochizuki N, Sawa H, Sato M, Nagashima K, Mizutani A, Matsuno A, Kiyokawa E, Matsuda M	R-Ras regulates exocytosis by Rgl2/Rlf-mediated activation of RalA on endosomes	Mol Biol Cell	18 (5)	1850-1860	2007
Seguchi O, Takashima S, Yamazaki S, Asakura M, Asano Y, Shintani Y, Wakeno M, Minamino T, Kondo H, Furukawa H, Nakamaru K, Naito A, Takahashi T, Ohtsuka T, Kawakami K, Isomura T, Kitamura S, Tomoike H, Mochizuki N, Kitakaze M	A cardiac myosin light chain kinase regulates sarcomere assembly in the vertebrate heart	J Clin Invest	117(10)	2812-2824	2007

VAP1 – snake venom homolog of mammalian ADAMs

Soichi Takeda

Department of Cardiac Physiology, National Cardiovascular Center Research Institute, Osaka, Japan

FUNCTIONAL CLASS

Enzyme; monozinc endopeptidase; a P-III class snake venom metalloproteinase (SVMP); a member of the reprolysin/adamalysin/ADAM (a disintegrin and metalloproteinase) family; clan MA(M) > family M12B > M12.186 (MEROPS classification, http://merops.sanger.ac.uk/).

OCCURRENCE

Vascular-apoptosis-inducing protein-1 (VAP1) is a P-III class SVMP that was isolated from western diamondback snake *Crotalus atrox* venom as a factor that induces apoptosis in cultured vascular endothelial cells (VECs).[1,2] Similar apoptotic SVMPs have been isolated from other hemorrhagic snake venoms.[3–8] SVMPs are classified into various groups (P-I to P-IV) according to their domain organization.[9,10] P-III SVMPs are composed of metalloproteinase (M), disintegrin-like (D), and cysteine-rich (C) domains, and display more potent hemorrhagic activity than P-I SVMPs, which contain only an M domain. In addition to apoptotic toxins, snake venoms contain a number of other SVMPs that play key roles in the pathologies associated with

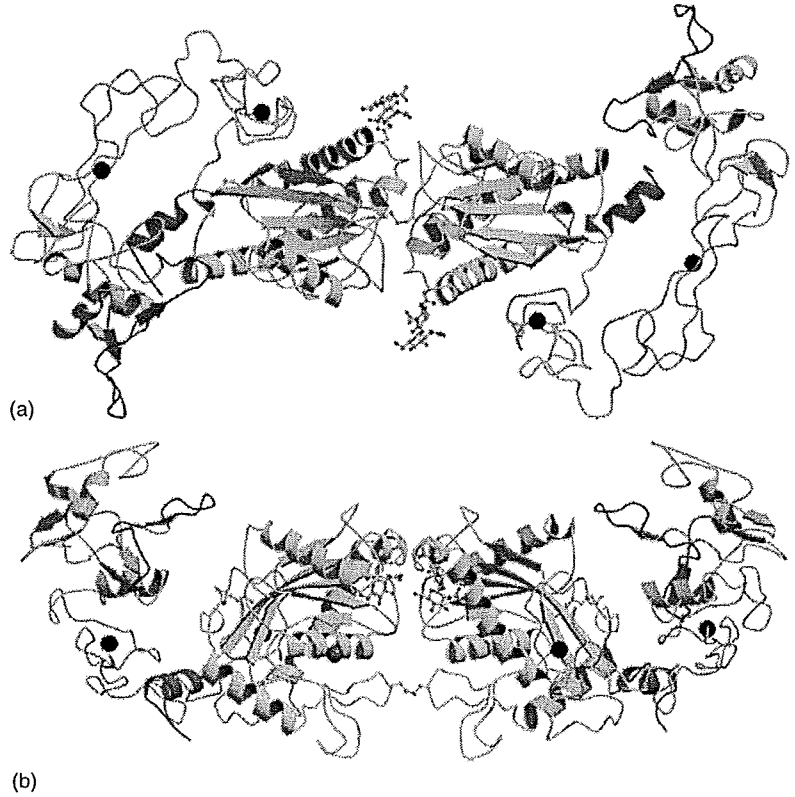

3D Structure Ribbon diagram of VAP1, viewed from the dimer axis (a) and from the direction perpendicular to the dimer axis (b), PDB code 2ERO. The structural subsegments are represented in different colors as follows: the h0-helix, M domain, linker, D_s, D_a, C_w, C_h segments, and HVR are shown in red, yellow, gray, cyan, pink, gray, light green and blue, respectively. Carbohydrate moieties linked to Asn218 are in ball-and-stick representation. The catalytic zinc ions and the calcium ions are represented by red and black spheres, respectively. Figures were generated using the MOLSCRIPT[83] and RASTER3D[84] programs.

envenoming, such as hemorrhage, edema, inflammation, and necrosis.[9–11] Mammalian ADAM family proteins are phylogenically related to P-III SVMPs and have a homologous metalloproteinase/disintegrin/cysteine-rich (MDC) domain architecture.[10,12] ADAMs and SVMPs, together with ADAMTSs (ADAM with thrombospondin type-1 motif),[13,14] constitute the adamalysin/reprolysin/ADAM subgroup of the metzincin clan of zinc proteinases.[15,16] ADAMs are primary type-I transmembrane proteins. In addition to the amino-terminal MDC domains, ADAMs have a transmembrane segment and a cytoplasmic region in their carboxy terminus.[12,17,18] The canonical ADAMs (see below) also have an epidermal growth factor (EGF)-like domain between the C domain and the transmembrane segment. ADAMs are widely expressed in multicellular organisms, including humans, mice, *Drosophila melanogaster*, and *Caenorhabditis elegans*. ADAMs are also expressed in *Schizosaccharomyces pombe* (but not in *Saccharomyces cerevisiae*).[19] Some ADAMs have alternatively spliced secreted forms in addition to the prototype transmembrane form.[20,21] There are 20 genes that encode human ADAMs and 37 genes that encode mouse ADAMs. The ADAMTS family is a branch of ADAMs, and constitutes a group of secreted proteinases that are expressed in a broad spectrum of species, ranging from humans to worms.[22] There are 19 known ADAMTS proteinases in vertebrates. A schematic representation of the domain structure of representatives of the adamalysin/reprolysin/ADAM family of proteins is shown in Figure 1.

BIOLOGICAL FUNCTION

SVMPs circulate within envenomed animals and are primarily responsible for local and systemic bleeding.

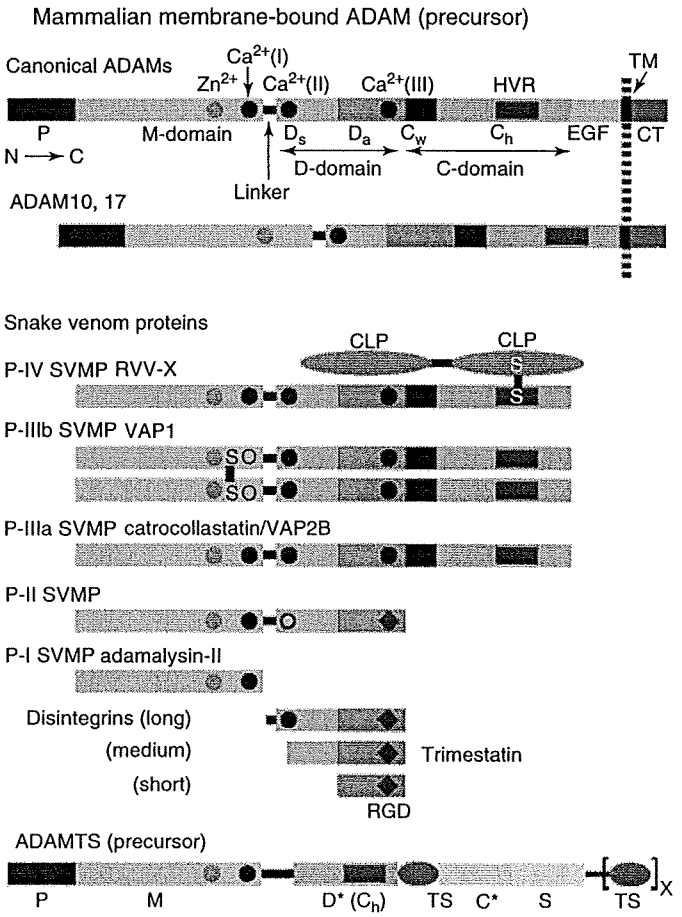

Figure 1 Schematic representation of the domain structures of ADAM/adamalysin/reprolysin family of proteins. Each domain or subsegment is colored as follows: the prodomain (Pro), transmembrane (TM), cytoplasmic region (CT), C-type lectin-like domain (CLP), thrombospondin type-1 domain (TS), and spacer (S) domain are in black, black, gray, brown, gray, and light green, respectively. The use of disintegrin-like (D) in the nomenclature of ADAMTS is a misnomer[23] as the D domain in ADAMTS-1 appears to be very similar in structure to the C_h segment of VAP1. Thus, the D domain of ADAMTSs is represented as the C_h segment. The C domain in ADAMTSs has no sequence homology to ADAMs, and is represented by a distinct color.

Some SVMPs do not possess hemorrhagic activity, but have other diverse functions attributable to them, such as fibrinogenase, prothrombin activating, or plate aggregation inhibitor activities.[10] VAP1 induces cell death in VECs in culture with the characteristic features of apoptosis, including fragmentation of cells and cleavage of DNA into a characteristic ladder pattern upon electrophoresis.[2] VAP1-induced apoptosis is dependent on its catalytic activity,[24] is inhibited by antibodies to integrins α3, α6, β1, and CD9 (cluster of differentiation antigen-9),[25] and involves activation of specific caspases.[26] However, the physiological target(s) of VAP1 and the underlying mechanism of VAP1-induced apoptosis remain elusive.

The first mammalian ADAMs, termed *fertilin* (hetero dimer of α- (ADAM1) and β-chain (ADAM2)), was identified in 1992 as surface molecules on sperm cells that are essential for fertilization.[27] Meltrins α (ADAM12), β (ADAM19), and γ (ADAM9) were isolated as molecules involved in myogenesis.[28] The best-characterized *in vivo* activity of mammalian ADAMs is their ectodomain sheddase activity. ADAM17 (tumor necrosis factor converting enzyme or TACE) was initially identified as the physiological convertase for tumor necrosis factor (TNF)-α.[29,30] ADAM10 (kuzbanian), which dictates the lateral inhibition of *Drosophila* neurogenesis,[31] releases Notch ligand delta[32] and Notch.[33] ADAM-mediated shedding can be activated by ligands for G-protein-coupled receptors (GPCRs). ADAMs have also been implicated in mitogenic events associated with EGF receptor transactivation by GPCRs.[34–36] However, in contrast to SVMPs and ADAMTSs, all of which are proteolytically active, only 60% of mammalian membrane-bound ADAMs contain the signature catalytic site motif HEXXHXXGXXHD (where X denotes any amino acid). The function of the proteinase-inactive ADAMs remains unclear. Aside from sheddase activity, ADAMs function in cell–cell and cell–matrix adhesion. The domains that are carboxy terminal to the M domain of ADAMs have been shown to exhibit adhesive activities in tissue culture.[37–39] ADAMs have been associated with numerous disease conditions including rheumatoid arthritis, Alzheimer's disease, heart disease, and cancer.[36,40,41] ADAM33 has been genetically linked to asthma and bronchial hyperresponsiveness in Caucasians.[42]

Disintegrins are small proteins (40–90 amino acids) that are generated, albeit not exclusively,[43] by proteolytic processing of larger precursor P-II SVMPs that are composed of M and D domains.[44,45] They typically possess an Arg-Gly-Asp (RGD) recognition sequence on an extended loop (disintegrin loop) that has been shown to inhibit platelet aggregation *via* integrin binding.[46,47] ADAMs are unique among the cell-surface proteins in that they possess a disintegrin-like sequence, which suggests that integrins are common receptors for ADAMs.[12,18,27,48] However, the RGD sequence in the ADAMs disintegrin-loop is usually replaced by XXCD, and therefore, the adhesive properties of the D domain are controversial.

AMINO ACID SEQUENCE INFORMATION

The VAP1 cDNA encodes a protein of 610 amino acid residues (EMBL database: AB042840). Mature VAP1 is a disulfide-bonded homodimer of polypeptide chains of 423 residues each. The signal sequence and the prodomain, which precede the M domain, are cleaved by posttranslational processing, and the mature protein contains only the MDC domain. The MDC domains of human ADAMs exhibit 30–40% sequence identity with VAP1.[49]

The prodomain of VAP1 contains a cysteine-containing sequence, PKMCGVT, which is thought to maintain the proteinase in a latent state, and is activated by a cysteine-switch mechanism.[50] The cysteine-containing sequence is conserved among the adamalysin/reprolysin/ADAM family proteins and the matrix metalloproteinases (MMP) of the metzincin clan of metalloproteinases. The mechanism of removal of the prodomain of VAP1 has not been clarified. The activation of some ADAMs has been shown to involve their own proteinase activity, while the others are believed to be activated by proprotein convertases (e.g. furin) in the secretary pathway.

PROTEIN PRODUCTION, PURIFICATION, AND MOLECULAR CHARACTERIZATION

VAP1 can be purified from the lyophilized powder of *C. atrox* venom by conventional liquid chromatography.[51] In the amino terminus of the M domain, Glu184 is modified to its pyro-form, and a carbohydrate chain is linked to the residue Asn218.[49]

VAP1 has a unique dimeric structure, and most adamalysin/reprolysin/ADAM family proteins do not appear to form VAP1-type dimers, as they lack the consensus QDHSK sequence (residues 320–324 in VAP1) and Cys365.[49] The consensus sequence and a cysteine residue at this position are found in other apoptotic P-III SVMPs, such as HV-1 (habu snake vascular-apoptosis-inducing protein-1),[4] halysase,[5] and VLAIP (*Vipera lebetina* apoptosis-inducing protein).[6] The VAP1-type dimers are categorized as the P-IIIb subclass of SVMPs, to distinguish them from the monomeric P-IIIa SVMPs.[10]

METAL CONTENT AND COFACTORS

There are one zinc and two calcium ions bound per VAP1 monomer, as shown by X-ray crystallography.[49] On the basis of the structures of VAP1 and the related proteins, and amino acid sequence alignment, the canonical ADAM MDC domains contain one zinc ion and three calcium ions. No other cofactors are present.

ACTIVITY AND INHIBITION TESTS

VAP1 degrades fibrinogen *in vitro*,[24] although the cleavage site(s) has not been identified. After incubation with either ethylenediaminetetraacetic acid (EDTA) or ethyleneglycol bis (2-aminoethyl ether) tetraacetic acid (EGTA), the ability of VAP1 to degrade fibrinogen and induce apoptosis in VECs is severely impaired.[24] Hydroxamic acid derivatives, such as GM6001 has been given as (*N*-[(2*R*)-2-(hydroxamidocarbonylmethyl)-4-methylpentanoyl]-L-tryptophan methylamide) also inhibit VAP1-induced VEC apoptosis. Therefore, the metalloproteinase activity of VAP1 appears to be involved in the induction of apoptosis by VAP1. Most of the hemorrhagic SVMPs degrade basal membrane component proteins[11]; however, the degradation activity of VAP1 toward those proteins *in vitro* is very weak.

The 12 human ADAMs (ADAM8, 9, 10, 12, 15, 17, 19, 20, 21, 28, 30, and 33) contain a catalytic signature sequence (HEXXHXXGXXHD), and most of them (with the exception of ADAM20, 21, and 30) have been shown to be proteolytically active.[12,17,18]

X-RAY AND NMR STRUCTURES

The first member of the adamalysin/reprolysin/ADAM family of proteinases for which the X-ray structure was determined was adamalysin II, a P-I SVMP from *Crotalus adamantus*.[52,53] Since then, crystal structures of seven P-I SVMPs have been published.[54–60] The structures of several disintegrins have been determined by X-ray crystallography[61–63] and NMR.[64–68] Although the crystallization papers of two P-III SVMPs, Jararhagin from *Bothrops jararaca* and AaH-IV from *Agkistrodon acutus* venoms, are available,[69,70] the three-dimensional structures have not been reported. The structures of seven mammalian proteins are currently available – the M domains of human ADAM17[71] and ADAM33,[72] the DC domains of bovine ADAM10,[73] the M domain of human ADAMTS-5,[74] and the MD domains of human ADAMTS-1,[23] ADAMTS-4, and ADAMTS-5.[75]

VAP1 was the first P-III SVMP structure to be resolved by X-ray crystallography.[49] The crystal structures of VAP1 have revealed an MDC domain architecture, which is shared by the mammalian ADAMs. Crystal structures of three different crystal forms of catrocollastatin/VAP2B, an apoptotic, monomeric class (P-IIIa) of SVMP[3,7] that has platelet-aggregation inhibitory activity,[76] have been determined.[77] A comparison of the six catrocollastatin/VAP2B structures and the structures of VAP1 reveals a dynamic, modular architecture of the MDC domains that may be important for the functions of adamalysin/reprolysin/ADAM family proteins.[77] The third MDC-containing SVMP for which the crystal structure was solved is RVV-X,[78] an unusual metalloproteinase that belongs to the P-IV class of SVMPs. Two C-type lectin-like chains are added posttranslationally to the C domain of P-III class SVMPs.[10,79–81] Although no mammalian ADAM MDC-domain crystal structures are currently available, electron microscopy of negative-stained recombinant ADAM12 with its prodomain revealed a four-leaf-clover shape, in which three of the four leaves represented the MDC domains.[82] Table 1 summarizes the adamalysin/reprolysin/ADAM family proteins currently entered into the Protein Data Bank.

Crystallization

VAP1 was crystallized in two distinct crystal forms using the sitting or hanging drop vapor diffusion methods.[49,51] Crystals were obtained with a reservoir solution that contained 15% polyethyleneglycol (PEG) 8000 and 100 mM sodium cacodylate at pH 6.5, with (orthorhombic form) or without (tetragonal form) 20 mM cobaltous chloride hexahydrate. The orthorhombic crystals belonged to space group $P2_12_12_1$ with $a = 86.7$ Å, $b = 93.3$ Å, $c = 137.7$ Å and one VAP1 dimer in the asymmetric unit. The tetragonal crystals belonged to space group $P4_12_12$ with $a = b = 93.9$ Å, $c = 244.8$ Å and one VAP1 dimer per asymmetric unit. Inhibitor-bound crystals were prepared by adding GM6001 to the drop with the orthorhombic crystal at a final concentration of 0.33 mM, followed by a 12-h incubation. Native structures were determined from crystals in the two distinct space groups at 2.5 Å resolution, and GM6001-bound structure was determined at 3.0 Å resolution.[49]

Like other proteins, adamalysin/reprolysin/ADAM family proteins are more prone to crystallize with inhibitors, which not only increase the thermal stability of the proteins[74] but also provide additional contacts with neighboring molecules in the crystalline lattice.[51,77,78]

MDC domains form a 'C shape'

The MDC domain architecture of VAP1 is shown in 3D structure and Figure 2(a) and (b). The M domains in the dimer are related by a noncrystallographic twofold axis, such that their active sites point in opposite directions, and an interchain disulfide bridge is formed between symmetry-related Cys365 residues. Each monomer has an almost identical structure except for the subdomain orientations. The M domain is followed by the D domain, which is further divided into two structurally distinct subsegments, the 'shoulder' (D_s) and the 'arm' (D_a) segments. The D_s segment protrudes from the M domain close to Ca^{2+} binding site I (see below), opposite the catalytic zinc ion. The C domain is subdivided into 'wrist' (C_w) and 'hand' (C_h) segments. Because of the curved structure of the $D_s/D_a/C_w/C_h$ segments, with the concave surface facing

Table 1 Selection of the 3D structures of ADAM/adamalysin/reprolysin family proteins currently deposited in the PDB

Protein	Domains	Method	PDB code	Reference
Snake venom proteins				
VAP1	MDC (homodimer)	X ray	2ERO, 2ERP, 2ERQ	49
Catrocollastatin/VAP2B	MDC	X ray	2DW0, 2DW1, 2DW2	75
RVV-X (russellysin)	MDC + 2CLPs	X ray	2E3X	76
Adamalysin II	M (P-I SVMP)	X ray	1AIG, 2AIG, 3AIG	52, 53
Atrolysin C	M (P-I SVMP)	X ray	1ATL, 1HTD	54
Acutolysin A	M (P-I SVMP)	X ray	1BSW, 1BUD	55
BaP1	M (P-I SVMP)	X ray	1ND1	56
H2	M (P-I SVMP)	X ray	1WNI	57
TM-3	M (P-I SVMP)	X ray	1KUF, 1KUG, 1KUI, 1KUK	58
Acutolysin C	M (P-I SVMP)	X ray	1QUA	59
FII	M (P-I SVMP)	X ray	1YP1	60
Trimestatin	Disintegrin	X ray	1J2L	61
Schistatin	Disintegrin (homodimer)	X ray	1RMR	62
Disintegrin (*Echis carinatus*)	Disintegrin (heterodimer)	X ray	1TEJ	63
Disintegrin (*Echis carinatus*)	Disintegrin (homodimer)	X ray	1Z1X	Unpublished
Kistrin	Disintegrin	NMR	1N4Y	67
Rhodostmin	Disintegrin	NMR	2PJF	Unpublished
Echistatin	Disintegrin	NMR	1RO3, 2ECH	65
Flavoridin	Disintegrin	NMR	1FVL	66
Obtustatin	Disintegrin	NMR	1MPZ	64
Salmosin	Disintegrin	NMR	1L3X	68
Mammalian proteins				
ADAM33	M	X ray	1R54, 1R55	72
ADAM17 (TACE)	M	X ray	1BKC	71
ADAM10	DC	X ray	2AO7	73
ADAMTS-5	M	X ray	3B8Z	74
ADAMTS-1	MD*	X ray	2JIH, 2V4B	23
ADAMTS-4	MD*	X ray	2RJP, 3B2Z	75
ADAMTS-5	MD*	X ray	2RJQ	75

* The use of disintegrin-like (D) domain in the nomenclature of ADAMTS is a misnomer.[23] The D-domain in ADAMTSs appears no structural similarity to the D-domain of ADAMs and SVMPs, and thus is represented as "D*".

the M domain, the overall appearance of the MDC domains is a C-shaped configuration. The distal portion of the C_h segment comes close to and faces the catalytic zinc ion in the M domain.

Metalloproteinase domain

The VAP1 M domain has as an oblate ellipsoidal shape with a notch in its flat side that creates a relatively small 'lower' domain and an 'upper' main molecular body in the 'standard' orientation,[15,52,85] wherein the active-site cleft extends horizontally across the M-domain surface to bind peptide substrates from left to right (Figure 2b). The catalytic zinc atom is located at the bottom of the cleft. The amino-terminal upper domain has a central core consisting of highly twisted five-stranded β-sheets and five α-helices. The amino-terminal h0 helix located on the h5 helix is unique to VAP1, and is not found, to date, in the structures of other family members. The curved β-sheets are parallel, with the exception of s4-strand, which faces the active-site cleft, and is sandwiched between helices h2 and h4 on the concave side and helix h3 on the convex side. The short helix h1 is located at an edge of the β-sheet. A topology diagram of the M domain is shown in Figure 2(c). The secondary structural arrangement is similar to other metzincins, such as astacin[85] and human neurophil collagenase (MMP-8),[86] except for a large insertion of helix h3 and the loop between strand s2 and helix h3. This insertion contributes to calcium binding site I (see below), which is unique in the adamalysin/reprolysin/ADAM family proteinases. The carboxy-terminal lower domain consists of helix h5 and an irregularly folded region. This irregular region is presumably important for substrate recognition because it forms, in part, the wall of the S1′ crevice, contains the 'Met-turn', and is stabilized by two conserved disulfide bridges (Cys350–Cys374 and Cys352–Cys357). A third highly conserved disulfide bridge (Cys310–Cys390)

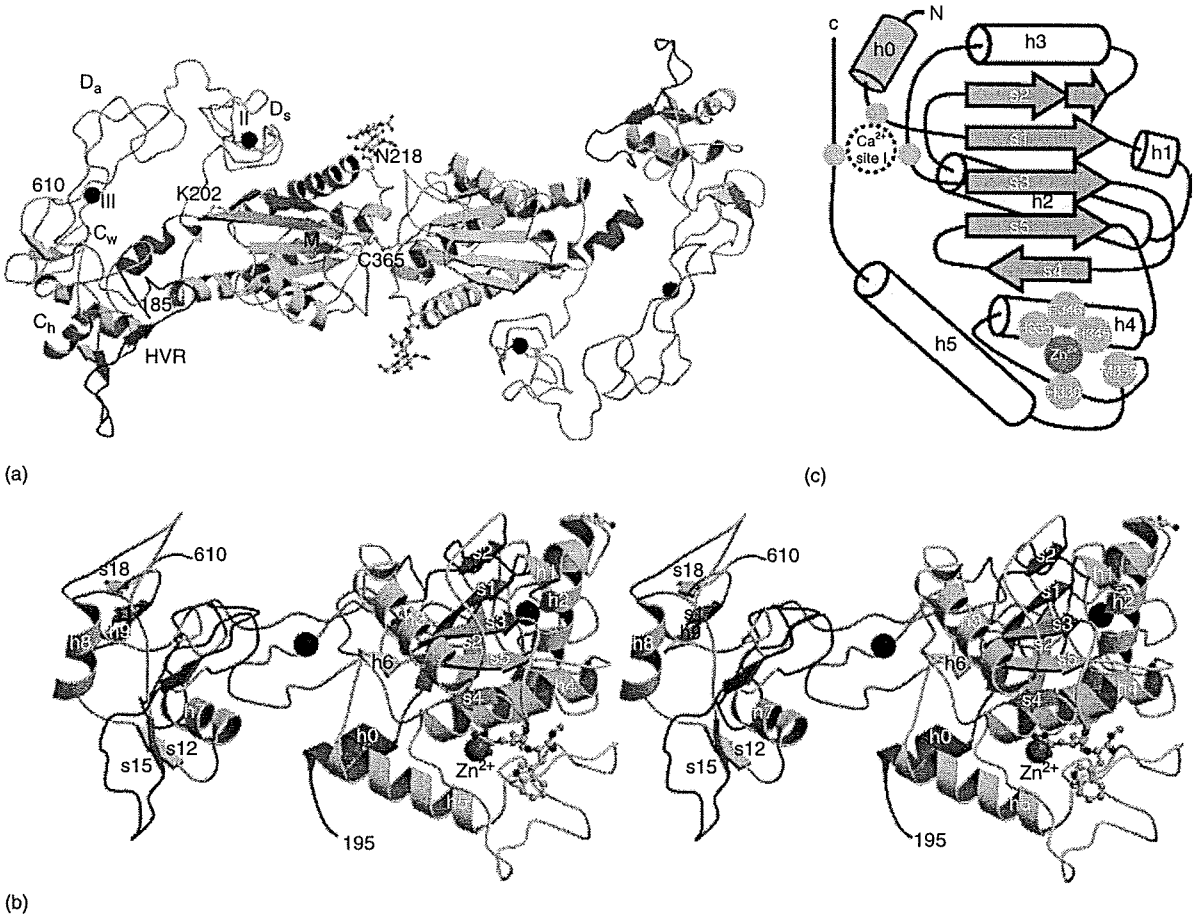

Figure 2 Ribbon structure of VAP1. (a) VAP1 dimer viewed from the twofold axis. The h0 helix, M domain, linker, D_s, D_a, C_w, C_h segments, and HVR are shown in red, yellow, gray, cyan, pink, gray, light green, and blue, respectively. Zinc and calcium ions are represented as red and black spheres, respectively. The carbohydrate moieties linked to Asn218 the calcium-mimetic Lys202 and bound GM6001 (in green) are in ball–stick representations; (b) stereo view of the VAP1 monomer in the standard orientation, nearly perpendicular to the view in (a); (c) topology diagram of the VAP1 M domain. Figures were generated using the MOLSCRIPT[83] and RASTER3D[84] programs.

connects the two subdomains close to Ca^{2+} binding site I. The M domain of VAP1 can be superposed with those of human ADAM33[72] and ADAM17[71] (Figure 3).

Arm structure

The VAP1 D domain is linked to the M domain by a short linker that allows variable orientation between the M domain and the D_s segment. The D_s and D_a segments consist largely of a series of turns and two short regions of antiparallel β-sheet, and constitute an elongated C-shaped arm structure together with the amino-terminal region of the C domain, the C_w segment (Figure 4(a)). The C_w segment consists of a pair of antiparallel β-strands and loops. It packs against the D_a segment on one side and against the carboxy-terminal β-sheet of the C_h segment on the other. There are three disulfide bridges in the D_s segment, three in the D_a segment, and one in the C_w segment. The subsegments are connected by single disulfide bridges. The number and spacing of the cysteine residues involved in these disulfide bridges are highly conserved among adamalysin/reprolysin/ADAM family proteins (Figure 4(c)).[10,44,49,77] Because there are few secondary structural elements, the disulfide bridges, together with bound calcium ions (see below), are essential for the structural rigidity of each segment of the C-shaped arm structure.

As predicted from its amino acid sequence, the structure of the D_a segment is similar to that of the RGD-containing disintegrin trimestatin (root mean square deviation (rmsd) of 1.24 Å),[61] with the exception of the disintegrin loop and the carboxy terminus of the D_a segment (Figure 4(b)). These two regions in disintegrins are highly mobile and are candidate sites for integrin binding.[65–67] Using isolated D domains or portions of them, numerous

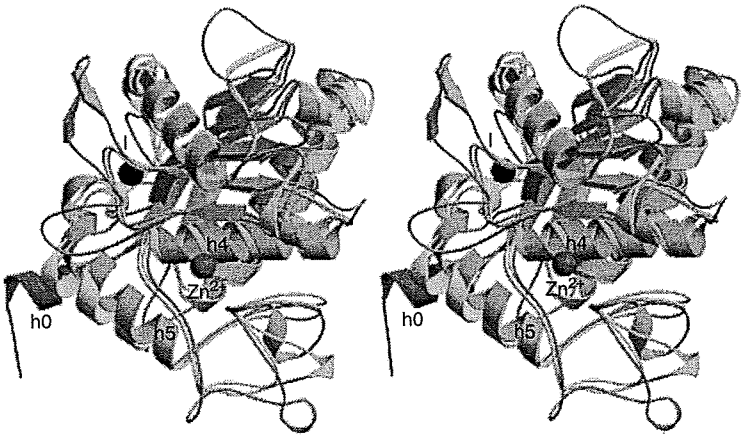

Figure 3 Stereo view of the superimposition of the M domains of VAP1 (yellow), ADAM33 (cyan), and ADAM10 (pink). The calcium ion bound to site I and the zinc ion in ADAM33 are represented by black and red spheres, respectively. The h0 helix in VAP1 is colored red.

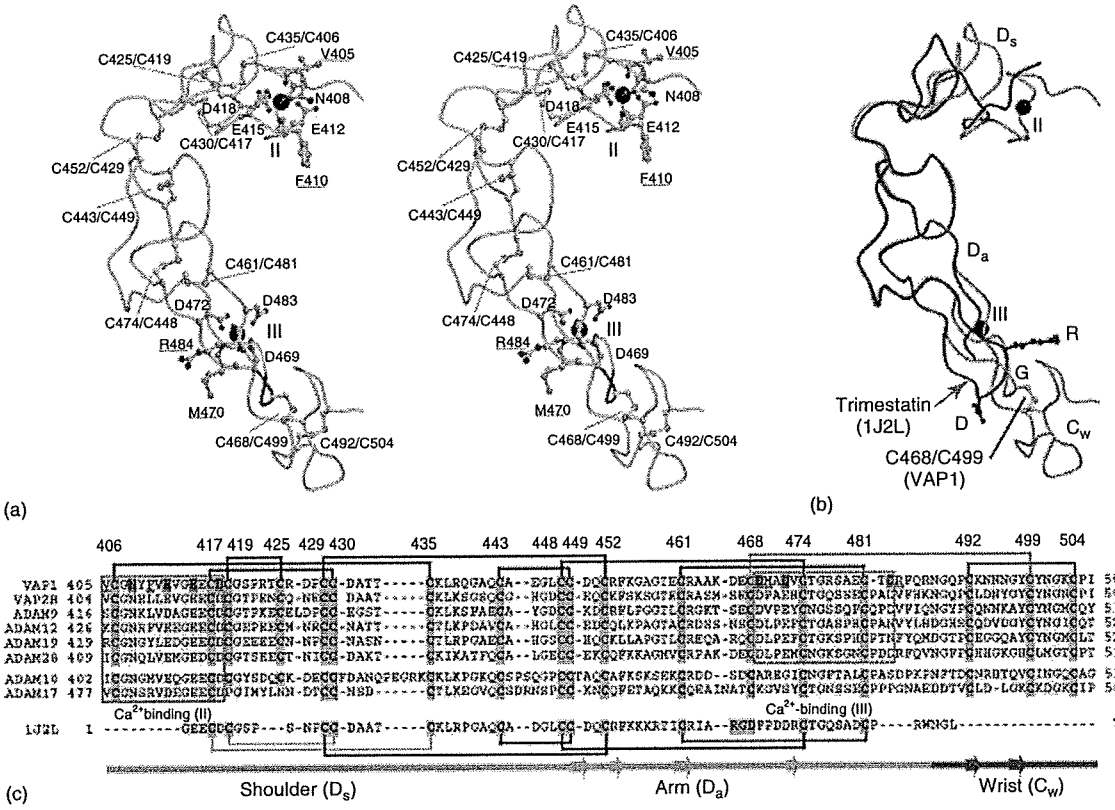

Figure 4 Arm structure of VAP1 (a) stereo diagram of the arm structure. The D_s, D_a, and C_w segments are in cyan, pink, and light green, respectively. The residues involved in calcium ion coordination and the disulfide bridges are shown in red and green, respectively. The carbonyl oxygen atoms of the residues that are involved in calcium coordination are underlined. Calcium ions are represented as black spheres. The disintegrin-loop (DECD) is in blue; (b) superimposition of the D_s segments of VAP1 and trimestatin (1J2L). Trimestatin and its RGD loop residues are shown in red and blue, respectively; and (c) amino acid sequence alignment of VAP1, trimestatin, and human ADAMs. The cysteinyl residues and conserved residues are shaded in pink and yellow, respectively. Disulfide bridges, secondary structures, and the boundary of the segments are shown schematically. The calcium binding sites are boxed in red, and the residues involved in calcium ion coordination are indicated. The National Center for Biotechnology Information (NCBI, http://www.ncbi.nlm.nih.gov/) accession numbers for the sequences are BAB18307 for VAP1, AAC59672 for VAP2B (catrocollastain/VAP2B), NP_003807 for ADAM9, AAC08703 for ADAM12, NP_075525 for ADAM19, NP_079496 for ADAM28, Z48579 for ADAM10, U69611 for ADAM17, and 1J2L for trimestatin. Figures were generated using the MOLSCRIPT[83] and RASTER3D[84] programs.

ADAMs, and P-III SVMPs have been shown to interact with integrins.[12,18,47,48] However, in VAP1, a bound calcium ion at site III forms a structural core that stabilizes the disintegrin-loop that is packed against the C_w segment. A disulfide bond (Cys468–Cys499) further stabilizes the continuous structure, which suggests that there is little intersegment flexibility. Cys468 is conserved among mammalian ADAMs and P-III SVMPs, which always contain a C domain. The structures of the DC domains of bovine ADAM10,[73] catrocollastain/VAP2B,[77] and RVV-X[78] also show a continuous D_a/C_w structure. These observations suggest that the disintegrin loop in ADAMs and P-III SVMPs is unavailable for protein binding due to steric hindrance.

Metal site geometries

Catalytic site (Zn^{2+})

VAP1 has a zinc-binding consensus sequence (HEXXHXXGXXH), which is characteristic of the metzincin superfamily.[15,16] The zinc ion is situated at the bottom of the catalytic cleft, and is tetrahedrally coordinated by the Nε2 atoms of the three consensus histidines, His335, His339, and His345, with bond distances of 2.0–2.2 Å. The coordination of the catalytic zinc atom is almost the same as in other members of this family. In GM6001-bound VAP1, the zinc ion is pentacoordinated by the two hydroxamate oxygen atoms and the Nε2 atoms of the three histidines (Figure 5).

Ca^{2+} binding site in the M domain (Ca^{2+} site I)

The MDC domain contains three potential Ca^{2+} binding sites. The structures of the M domain of ADAM33[72] and

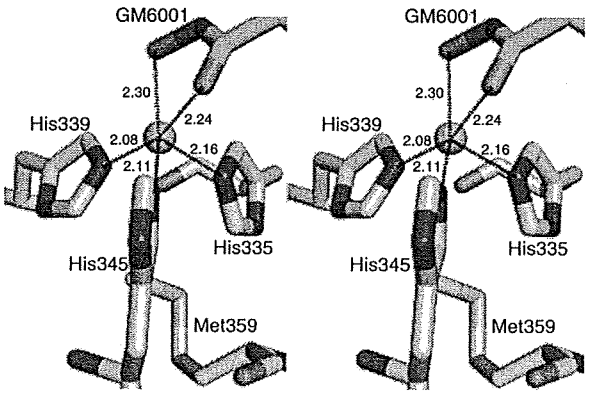

Figure 5 Stereo diagram of the catalytic zinc (pink sphere) of the VAP1–GM6001 complex (PDB code 2ERQ). The hydroxamic acid group of bound GM6001 and three histidine ligands are shown, along with the Zn–N/O distances (angstrom). The figure was generated using PyMOL.[87]

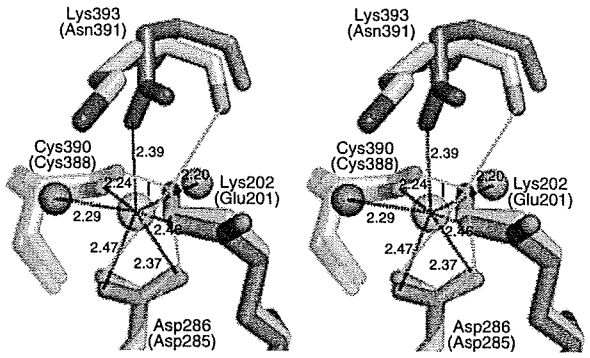

Figure 6 Stereo diagram of calcium binding site I of VAP1 (gray) superposed on that of catrocollastain/VAP2B (blue). The Ca^{2+}/N–O distances (angstrom) are indicated. The figure was generated using PyMOL.[87] The ammonium group of Lys202 in VAP1 occupies the position of the calcium ion in catrocollastatin/VAP2B.

of other P-I SVMPs[52,53,55] suggest that most ADAMs have a Ca^{2+} binding site (designated Ca^{2+} binding site I) that is in opposition to the active-site cleft close to the crossover point of the amino-terminal and carboxy-terminal segments of the M domain. In catrocollastatin/VAP2B, this Ca^{2+} ion is coordinated by the side chains of Asp285, Asn391, and Glu201, the backbone carbonyl oxygen of Cys388, and two water molecules in a pentagonal bipyramidal arrangement.[77] The three side chains that coordinate the Ca^{2+} ion are largely conserved among ADAMs and SVMPs. However, in VAP1, Glu and Asn are replaced by Lys202 and Lys392, respectively, and the distal ammonium group of Lys202 substitutes for the Ca^{2+} ion (Figure 6). Replacement of the calcium-coordinating glutamate residue with lysine is also observed in several ADAMs (e.g. human ADAMs16, 25, and 38–40). The high degree of conservation of residues involved in calcium binding and the presence of mimetic calcium binding might reflect the importance of this region for the structural link between the M and D_s domains. A protective role for calcium against auto proteolysis in the linker region has also been reported,[45,53,88] and the linker region is usually removed from P-I SVMPs posttranslationally.[89] ADAM17[71] and, presumably, ADAM10 do not possess this calcium binding site. These two ADAMs are not typical members of the mammalian family of ADAMs. They also lack Ca^{2+} binding site III, and lack an EGF domain.

Ca^{2+} sites in the D_s- and D_a segments

The structure of both the D_s and D_a segments revealed Ca^{2+} binding sites[49] that were not predicted by protein sequence. In the D_s segment, side-chain oxygen atoms of residues Asn408, Glu412, Glu415, and Asp418, and main-chain oxygen atoms of Val405 and Phe410 are

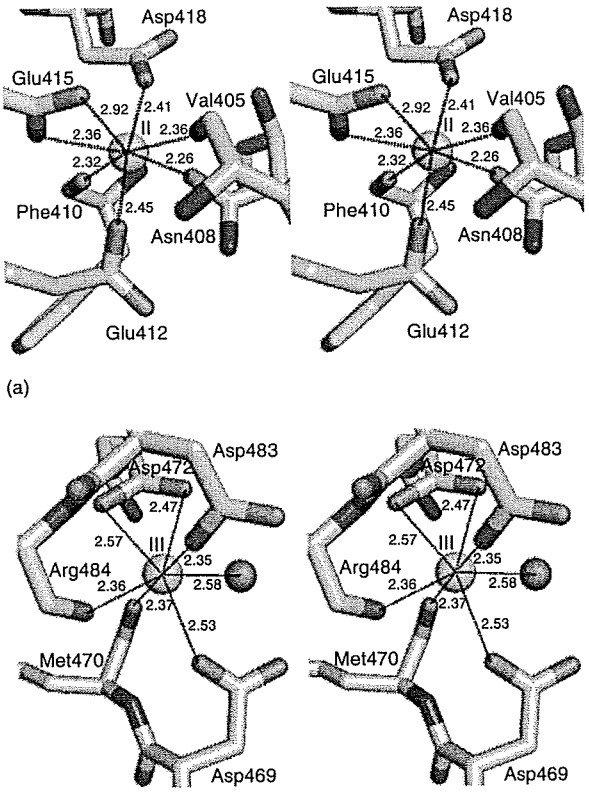

Figure 7 Stereo diagram of bound calcium ions in the (a) D_s segment (site II) and in the (b) D_a segment (site III) of VAP1. The Ca^{2+}–O distances (angstrom) are indicated. The figure was generated using PyMOL.[87]

involved in pentagonal bipyramidal coordination (hepta-coordination) of Ca^{2+} binding site II (Figure 7(a)). Of note, these residues are strictly conserved among all known mammalian ADAMs and P-III SVMPs.[49,77] Side-chain oxygen atoms of Asp469, Asp472, and Asp483, and the main-chain carbonyl oxygen atoms of Met470 and Arg484 coordinate the binding of a Ca^{2+} ion at the corners of a pentagonal bipyramid, and constitute Ca^{2+} binding site III in the D_a segment (Figure 7(b)). These residues are highly conserved among mammalian ADAMs, with the exception of ADAM10 and ADAM17.[49,77]

Hand (C_h segment) structure and hypervariable region (HVR)

The core of the carboxy-terminal region of the VAP1 C domain, the C_h segment, is an α/β fold structure that consists of two antiparallel β-strands packed against two of the three α-helices, and five disulfide bonds (Cys511–Cys561, Cys526–Cys572, Cys539–Cys549, Cys556–Cys598, and Cys592–Cys603) (Figure 8(a)). The C_h segment of VAP1 has a novel and unique fold with no structural homology to other known proteins, with the exception of the corresponding segment of ADAM10[73] and ADAMTS-1[23] (see below).

The loop encompasses residues 562–583, and extends across the central region of the C_h segment. It is the region in which the ADAM sequences are most divergent and variable in length (11–55 aa) (Figure 8(e)). We have designated this the hypervariable region (HVR).[49] In all the crystal forms of VAP1 and catrocollastatin/VAP2B, the HVR is involved in crystal packing, and forms a short antiparallel β-strand in the center that participates in a 'handshake' with the HVR of a neighboring molecule.[49,77] The structure of the HVR is stabilized mainly by interchain interactions. However, while there are no main chain–main chain hydrogen bonds between residues 574–584 and the remainder of the C_h segment, a water-mediated hydrogen bond network helps stabilize the HVR structure. Therefore, it appears that the HVR β-strand might be formed by an induced fit mechanism upon the association of the C_h segment, and that the conserved disulfide bridge (Cys526–Cys572) stabilizes the structure when the HVR is isolated in solution. Some ADAMs possess a putative fusion peptide sequence in this segment that is typical of viral fusion proteins[27,28]; however, its role in the actual fusion process has not been experimentally demonstrated.

The HVR is located at the distal end of the C-shaped MDC domain, and points toward the M-domain catalytic site, with a distance of ~4 nm between them. It has been suggested that the C domain is an adhesion domain with potential protein–protein and protein–matrix binding surfaces. However, most of the studies that implicate this region in heterologous interactions have not identified specific regions of the C domain that are involved, and the molecular mechanism of recognition is not well understood. Different ADAMs and SVMPs have distinct HVR sequences, which results in their having distinct surface features that may play a role in binding specificity. The VAP1 structure indicates that the HVR may interact with other proteins, bringing them toward the M-domain catalytic site where they can interact directly with the catalytic cleft. These observations suggest that the HVR of both ADAMs and SVMPs could be an exosite for the cleavage of certain cell-surface molecules; that is, it may directly interact with target molecules or their associated proteins that are processed by the catalytic site. The D domain is located opposite and apart from the catalytic site, and thus, might function primarily as a scaffold that positions the catalytic site and the exosite in the proper position and orientation.

Comparison to the related structures

ADAM 10 and ADAMTS-1 C_h domains

ADAM10 and ADAM17 show less sequence similarity, particularly in the C domain, to the other canonical

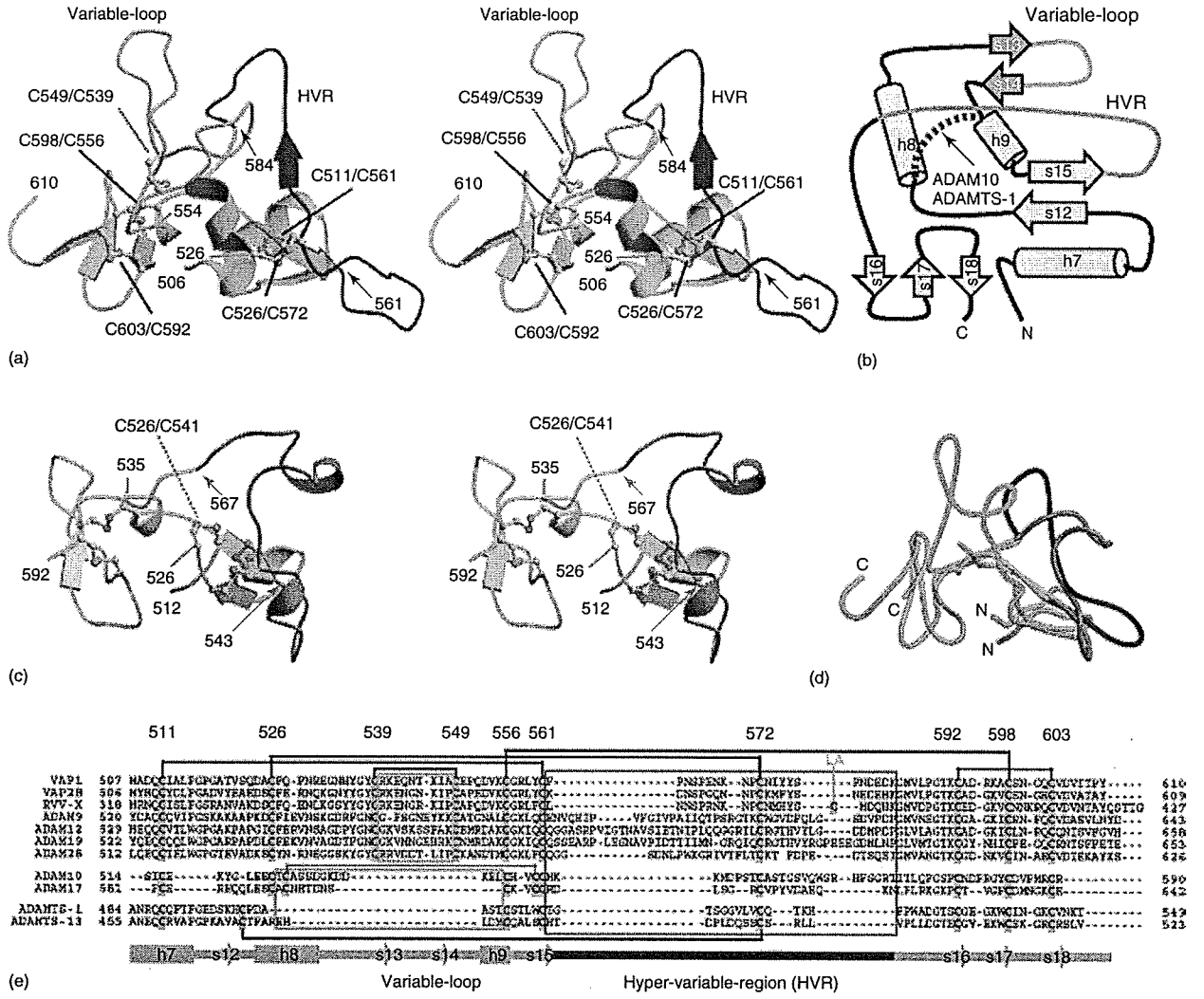

Figure 8 Structures of the hand segment (C_h segment) of VAP1 and human ADAM10. (a) Ribbon diagram of the VAP1 C_h segment in stereo. The HVR is shown in blue. The common scaffold of VAP1, ADAM10, and ADAMTS-1 is shown in cyan, and the segment lacking in ADAM10 is shown in light green. Disulfide bridges are indicated; (b) topology diagram of the C_h segment of VAP1; (c) ribbon representation of the C_h segment of ADAM10 in stereo. The HVR is shown in red. The numbering of the amino acids of ADAM10 (bovine) were changed to that of human; (d) superimposition of the C_h segments of VAP1 and ADAM10. The colors are as described for (a) and (c); and (e) structure-based alignment of the C_h segments of SVMPs, human ADAMs, and human ADAMTSs. Secondary structures of VAP1 and the disulfide bridges are represented schematically.

ADAMs. A comparison of the bovine ADAM10 DC domain structure ($ADAM10_{D+C}$)[73] and that of VAP1 reveals that these two proteins share a continuous D_a/C_w structure and C_h segment scaffold[49] (Figure 8(a–c)). The crystal structure of the MD domains of the human ADAMTS-1 has recently been determined, and it shows that the previously named disintegrin-like domain of ADAMTS-1 appears to be very similar in structure to the C_h segment of VAP1 (rmsd of 1.1 Å for 52 Cα atom positions), despite low sequence identity (~16%) between the two molecules.[23] The locations of the four disulfide bonds within the C_h segment are conserved among VAP1, ADAM10, and ADAMTS-1, which enabled us to align the three sequences. Figure 8(e) shows the sequence alignment of a selected subset of human ADAMs, ADAMTSs, and SVMPs. ADAM10 and ADAMTS-1 lack helix h8 and the variable loop that protrudes from VAP1, and have different HVR structures (the amino-terminal region of the HVR of ADAMTS-1 is disordered and has not been included in the model[23]). ADAMTSs lack the entire $D_s/D_a/C_w$ segments and their C_h segment is connected to the M domain by a connector loop (22 residues in ADAMTS-1) that wraps around the back of the M domain, resulting in a drastically different position of the C_h segment relative to the M domain compared to VAP1. ADAM10 also has a different spatial arrangement of the M and C_h

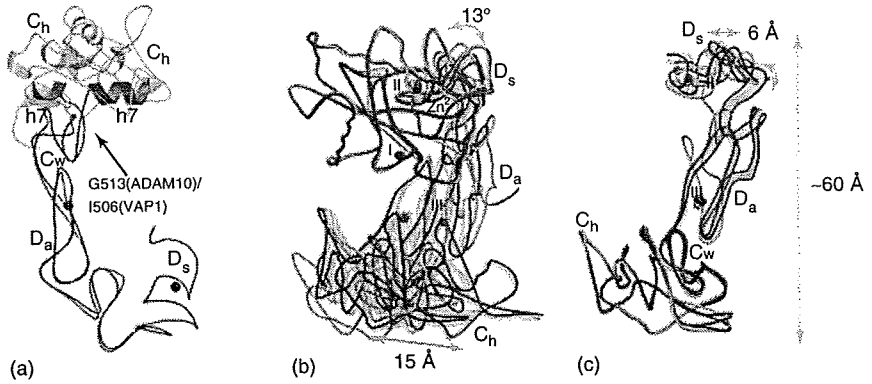

Figure 9 Mobility of the subdomains of VAP1, ADAM10, and catrocollastatin/VAP2B. (a) Superimposition of the D_a segments of ADAM10 and VAP1. The $D_s/D_a/C_w$ segments and helix h7 helix of VAP1 and ADAM10 are shown in blue and red, respectively. The C_h segments of VAP1 and ADAM10 are shown in cyan and pink, respectively. The arrow indicates the pivot point between the C_w and C_h segments. Bound calcium ions in VAP1 are shown as black spheres. Superposition of (b) the M domain and; (c) the C_h segments of the six structures of catrocollastatin/VAP2B and VAP1 monomer structure. Two representative catrocollastatin/VAP2B molecules are shown in blue and red, the other four catrocollastatin/VAP2B molecules are shown in gray, and VAP1 is in green. The zinc ion bound to the red molecule is shown as a yellow sphere. The calcium ions bound to the red and the blue catrocollastain/VAP2B molecules and VAP1 are shown as red, blue, and green spheres, respectively.

domains, primarily due to a different orientation between the C_w and C_h segments (Figure 9(a)). The possibility that different ADAMs have distinct C_w/C_h orientations remains to be determined. While most of the membrane-bound ADAMs have an EGF module between the C domain and the transmembrane segment, the ADAM10 C domain is separated from the cell membrane by only 26 residues, which are likely to be disordered.[73]

Catrocollastatin/VAP2B

The structures of catrocollastatin/VAP2B determined in three different crystal forms[77] are the first reported structures of a member of the monomeric class of MDC-domain-containing proteins of the adamalysin/reprolysin/ADAM family. The overall structure of catarocollastatin/VAP2B showed good agreement with each monomer of VAP1, and the structure of each segment was nearly identical between the molecules (Figure 9(b) and (c)). However the relative orientation of the subdomains was quite variable. Comparison of the six catrocollastatin/VAP2B monomer structures and the four VAP1 monomer structures derived from different crystal forms revealed a dynamic, modular architecture of the MDC domain of this family of proteins.[77] The largest difference was observed when the M domains of the six catrocollastatin/VAP2B molecules were superimposed (Figure 9(b)). The arm portion was rotated by approximately 13° relative to the M domain, bringing about a 15-Å displacement at the distal end of the C_h segment. A bulky hydrophobic residue (Leu, Phe, or Tyr) at position 408 is highly conserved among adamalysin/reprolysin/ADAM family proteins. The side chain of Leu408 in catrocollastatin/VAP2B functions as a universal joint (shoulder joint) that allows the D_s segment to adopt various orientations with respect to the M domain.[77] Intrinsic flexibility may be important for fine-tuning substrate recognition, and adjusting the spatial alignment of the catalytic and adhesion sites during the catalysis.

Structure of RVV-X

The coagulation factor X activator from Russell's viper venom (RVV-X, russellysin) is a unique metalloproteinase of the P-IV class of SVMPs that is composed of an MDC-domain-containing heavy chain and two C-type lectin-like light chains.[10,79–81] RVV-X specifically activates factor X by cleaving the Arg194–Ile195 bond in factor X, which is also cleaved by physiological convertases.[90] Cleavage removes the heavily glycosylated amino-terminal 52 residues (active peptide, or AP) of the factor X heavy chain, which results in exposure of the active site. Activated factor X (factor Xa) in turn converts prothrombin to thrombin, which ultimately leads to formation of a hemostatic plug.

The crystal structure of RVV-X resembles a hook–spanner–wrench configuration, in which the MD domains constitute a hook, and the rest of the molecule forms a handle (Figure 10(a)).[77] The two homologous light chains have a fold similar to the carbohydrate-recognition domain (CRD) of rat mannose binding protein (MBP),[91] but they form an intertwined dimer, in which the central portion of each chain projects toward the adjoining subunit. The RVV-X heavy chain has a unique cysteine residue (Cys389) in the middle of the HVR. Cys389 forms a disulfide bond with the carboxy-terminal cysteine residue of one of the light chains, light chain A (LA). In addition to

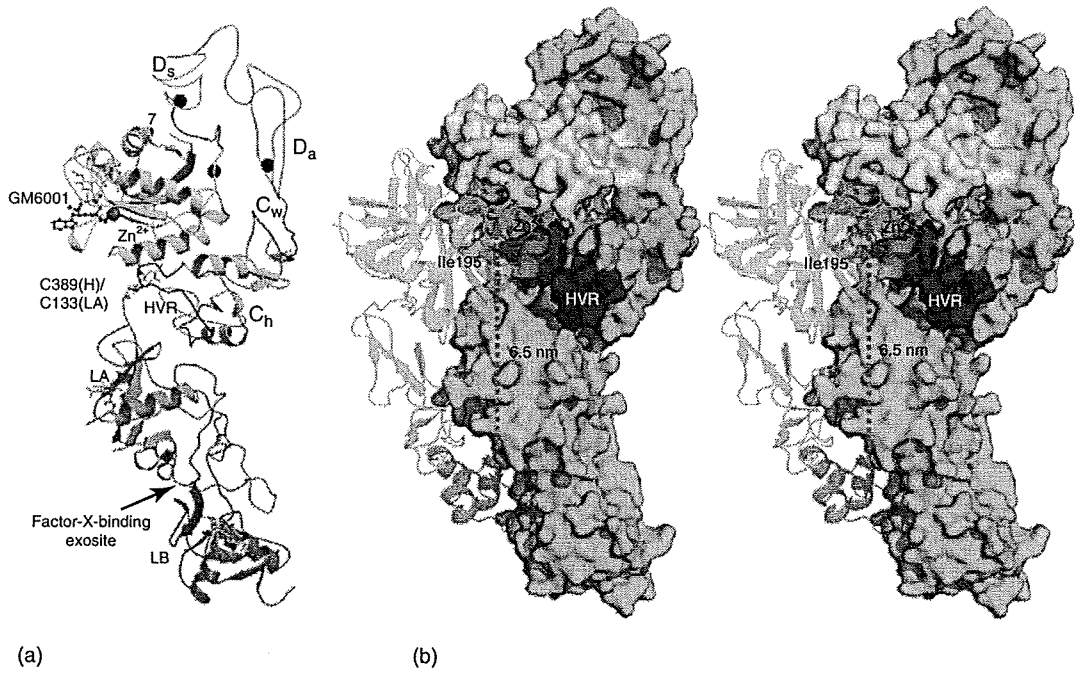

Figure 10 Structure of RVV-X and the factor-Xa docking model. (a) Crystal structure of RVV-X. Each segment of the RVV-X heavy chain is colored as described for VAP1 in Figure 2. Light chain A and B are colored in orange and magenta, respectively. The disulfide bridge between Cys389 in the heavy chain and Cys133 in light chain A, the carbohydrate moieties (in green) linked to asparagine residues, and GM6001 (in magenta) are shown in ball-and-stick representations. Bound calcium and zinc ions are represented as black and red spheres, respectively; (b) factor Xa docking model in stereo. The molecular surface of RVV-X is colored as for (a). Factor Xa is shown in ribbon representation. Ile195 (in stick representation) and the amino-terminal region of the factor Xa heavy chain are shown in magenta. Because the structure of the factor X zymogen is currently unavailable, the model was constructed on the basis of the factor-Xa crystal structures (1XKA and 1IOD).[78] In the factor Xa structure, the amino terminus of the heavy chain is buried within the protein. However, in the zymogen, the intact scissile peptide bond (Arg194–Ile195) must be situated on the molecular surface, as in the equivalent segments of other serine proteinase zymogen structures.

this interchain disulfide bond, the HVR and surrounding residues are engaged in multiple hydrophobic interactions and hydrogen bonds, which further stabilize the continuous C_h/LA structure. The RVV-X structure represents the first example of HVR-mediated protein–protein interactions in the adamalysin/reprolysin/ADAM family proteins.

The structure of the RVV-X light chains is quite similar to that of the factor X-binding protein (X-bp) from *Deinagkistrodon actus* venom, as determined in complex with the γ-carboxyglutamic acid (Gla) domain of factor X.[92] This structural similarity and the previous biochemical observations[81] suggest that the concave cleft created between the two light chains in RVV-X may function as an exosite for factor X. A 6.5 nm separation between the catalytic site and a putative Gla-domain-binding exosite suggests the docking model for factor X (Figure 10(b)).[78] The active-site zinc atom and Ile195 of factor Xa are 16 Å apart because the two molecules are positioned as rigid bodies without any contacts. Intrinsic flexibility between the segments of the RVV-X heavy chain, and conformational changes upon association of RVV-X and factor X zymogen, may allow the catalytic site of RVV-X to interact directly with the bond between Arg194–Ile195 of factor X in solution. The relatively large separation between the catalytic site and the exosite may explain the high specificity of RVV-X for factor X.

The VAP1 structure suggests a model in which the HVR constitutes an exosite that captures target or associated proteins that are then processed by the catalytic site.[49] The RVV-X structure[78] is consistent with this model and provides additional insights into the molecular basis of target recognition and proteolysis by ADAM/adamalysin/reprolysin proteinases. The fold adaptation of the RVV-X structure is also a good example of evolutionary gain of function by multi-subunit proteins for the binding of ligands.

FUNCTIONAL ASPECTS

C-domain-mediated protein–protein interactions

ADAM family proteins are widely distributed and constitute major membrane-bound sheddases that are involved in the proteolysis of cell-surface-protein ectodomains for

cell–cell communications. As such, they have emerged as potential therapeutic targets for various disease conditions. The P-III SVMPs are the most potent hemorrhagins and constitute key toxins in venom-induced pathologies. Thus, they are important targets for antivenom therapeutics. However, the physiological targets of ADAMs and SVMPs and the molecular mechanism of target recognition are poorly understood. The structures of VAP1 and related proteins highlight the potential roles of the C domain in protein–protein interactions.

There is mounting experimental evidence that C domains mediate protein–protein interactions. Peptides encompassing the HVR and the hydrophobic ridge from jararhagin and atrolysin-A (P-III SVMPs from *C. atrox* venom) interfere with platelet interaction and collagen binding.[93] Catrocollastatin-C and jararhagin-C, which are proteolytic products (DC-domain fragments) of catrocollastatin/VAP2B and jararhagin, respectively, have been shown to inhibit collagen-induced platelet aggregation.[94,95] Jararhagin-C also activates early events in the inflammatory response, such as leukocyte rolling and proinflammatory cytokine release.[96] Recombinant atrolysin-A C domain (A/C) specifically binds collagen type I and von Willebrand factor (vWF), and blocks collagen–vWF interactions.[97,98] It also binds to the von Willebrand factor A (VWA)-domain-containing extracellular matrix (ECM) proteins collagen XII and XIV, and matrilins 1, 3, and 4.[99] Binding of vWF in solution to immobilized A/C was inhibited by ristocetin, and preincubation of platelets with A/C abolished ristocetin/vWF-induced platelet aggregation, which indicates that the interaction of A/C with vWF is mediated by the VWA1 domain.[100] Two peptide sequences have been identified in the C domain of jararhagin that bind to vWF and block C-domain binding.[101] On the basis of the structures of VAP1 and catrocollastain/VAP2B, the Jar6 peptide (corresponding to catrocollastatin/VAP2B residues ^{547}PCAPEDVKCG^{556}) is located on the surface of the C domain, and thus could play a role in protein–protein interactions. ADAM12 interacts with cell-surface syndecan through its C domain and mediates integrin-dependent cell spreading.[37] The DC domain of ADAM13 has been implicated in cell migration events,[102] and binds to the ECM proteins laminin and fibronectin.[38] It should be noted, however, that most of these studies do not identify a specific region of the C domain that is involved in these interactions, and so the molecular mechanisms of recognition remain to be elucidated.

Several studies have indicated that the ADAMs' C domain can influence proteolytic activity. The C domain of ADAM13 was found to be the major determinant of specific developmental events that are mediated by the proteolytic activity of ADAM13.[103] Ectodomain shedding of interleukin-1 R-II by ADAM17 (TACE) requires the DC domains, whereas tumor necrosis factor (TNF) and p75 tumor necrosis factor receptor (TNFR) shedding by ADAM17 requires only the tethered M domain.[104] The acidic surface pocket in the ADAM10 C domain serves as a binding site for the ephrin-A5/EphA3 complex in ADAM10-mediated ephrin-A5 proteolysis.[22] Jararhagin cleaves vWF at sites adjacent to the VWA1 domain, and digestion is completely inhibited by the A/C and catrocollastatin-C.[100]

ACKNOWLEDGEMENTS

The author is indebted to T. Igarashi, Y. Ohishi, M. Tomisako, and S. Araki, who made essential contributions to the elucidation of the structures of VAP1, catrocollastatin/VAP2B, and RVV-X, and to H. Mori for support and encouragement. The financial support of the Ministry of Education, Science, Sports, and Culture, Grant-in-aid for Scientific Research B-19370047-2007, and Health and Labor Science Research Grants, and grants from the Mitsubishi Pharma Research Foundation and the Astellas Foundation for Research on Metabolic Disorders are kindly acknowledged.

REFERENCES

1 S Araki, T Ishida, T Yamamoto, K Kaji and H Hayashi, *Biochem Biophys Res Commun*, **190**, 148–53 (1993).
2 S Masuda, S Araki, T Yamamoto, K Kaji and H Hayashi, *Biochem Biophys Res Commun*, **235**, 59–63 (1997).
3 S Masuda, H Hayashi and S Araki, *Eur J Biochem*, **253**, 36–41 (1998).
4 S Masuda, H Hayashi, H Atoda, T Morita and S Araki, *Eur J Biochem*, **268**, 3339–45 (2001).
5 WK You, HJ Seo, KH Chung and DS Kim, *J Biochem (Tokyo)*, **134**, 739–49 (2003).
6 K Trummal, K Tonismagi, E Siigur, A Aaspollu, A Lopp, T Sillat, R Saat, L Kasak, I Tammiste, P Kogerman, N Kalkkinen and J Siigur, *Toxicon*, **46**, 46–61 (2005).
7 S Masuda, H Maeda, JY Miao, H Hayashi and S Araki, *Endothelium*, **14**, 89–96 (2007).
8 I Tanjoni, R Weinlich, MS Della-Casa, PB Clissa, RF Saldanha-Gama, MS de Freitas, C Barja-Fidalgo, GP Amarante-Mendes and AM Moura-da-Silva, *Apoptosis*, **10**, 851–61 (2005).
9 JB Bjarnason and JW Fox, *Methods Enzymol*, **248**, 345–68 (1995).
10 JW Fox and SM Serrano, *Toxicon*, **45**, 969–85 (2005).
11 JM Gutierrez, A Rucavado, T Escalante and C Diaz, *Toxicon*, **45**, 997–1011 (2005).
12 JM White, L Bidges, D DeSimone, M Tomczuk and T Wolfsberg, in NM Hooper and U Lendeckel (eds.), *The ADAM Family of Proteases*, Springer, Dordrecht (2005).
13 K Kuno, N Kanada, E Nakashima, F Fujiki, F Ichimura and K Matsushima, *J Biol Chem*, **272**, 556–62 (1997).
14 BL Tang and W Hong, *FEBS Lett*, **445**, 223–25 (1999).
15 FX Gomis-Ruth, *Mol Biotechnol*, **24**, 157–202 (2003).
16 W Bode, FX Gomis-Ruth and W Stockler, *FEBS Lett*, **331**, 134–40 (1993).
17 DF Seals and SA Courtneidge, *Genes Dev*, **17**, 7–30 (2003).
18 JM White, *Curr Opin Cell Biol*, **15**, 598–606 (2003).

19 T Nakamura, H Abe, A Hirata and C Shimoda, *Eukaryot Cell*, **3**, 27–39 (2004).

20 BJ Gilpin, F Loechel, MG Mattei, E Engvall, R Albrechtsen and UM Wewer, *J Biol Chem*, **273**, 157–66 (1998).

21 CM Roberts, PH Tani, LC Bridges, Z Laszik and RD Bowditch, *J Biol Chem*, **274**, 29251–59 (1999).

22 GC Jones and GP Riley, *Arthritis Res Ther*, **7**, 160–69 (2005).

23 S Gerhardt, G Hassall, P Hawtin, E McCall, L Flavell, C Minshull, D Hargreaves, A Ting, RA Pauptit, AE Parker and WM Abbott, *J Mol Biol*, **373**, 891–902 (2007).

24 S Masuda, T Ohta, K Kaji, JW Fox, H Hayashi and S Araki, *Biochem Biophys Res Commun*, **278**, 197–204 (2000).

25 S Araki, S Masuda, H Maeda, MJ Ying and H Hayashi, *Toxicon*, **40**, 535–42 (2002).

26 J Maruyama, H Hayashi, J Miao, H Sawada and S Araki, *Toxicon*, **46**, 1–6 (2005).

27 CP Blobel, TG Wolfsberg, CW Turck, DG Myles, P Primakoff and JM White, *Nature*, **356**, 248–52 (1992).

28 T Yagami-Hiromasa, T Sato, T Kurisaki, K Kamijo, Y Nabeshima and A Fujisawa-Sehara, *Nature*, **377**, 652–56 (1995).

29 RA Black, CT Rauch, CJ Kozlosky, JJ Peschon, JL Slack, MF Wolfson, BJ Castner, KL Stocking, P Reddy, S Srinivasan, N Nelson, N Boiani, KA Schooley, M Gerhart, R Davis, JN Fitzner, RS Johnson, RJ Paxton, CJ March and DP Cerretti, *Nature*, **385**, 729–33 (1997).

30 ML Moss, SL Jin, ME Milla, DM Bickett, W Burkhart, HL Carter, WJ Chen, WC Clay, JR Didsbury, D Hassler, CR Hoffman, TA Kost, MH Lambert, MA Leesnitzer, P McCauley, G McGeehan, J Mitchell, M Moyer, G Pahel, W Rocque, LK Overton, F Schoenen, T Seaton, JL Su, J Warner, D Willard and JD Becherer, *Nature*, **385**, 733–36 (1997).

31 J Rooke, D Pan, T Xu and GM Rubin, *Science*, **273**, 1227–31 (1996).

32 H Qi, MD Rand, X Wu, N Sestan, W Wang, P Rakic, T Xu and S Artavanis-Tsakonas, *Science*, **283**, 91–94 (1999).

33 D Pan and GM Rubin, *Cell*, **90**, 271–80 (1997).

34 N Prenzel, E Zwick, H Daub, M Leserer, R Abraham, C Wallasch and A Ullrich, *Nature*, **402**, 884–88 (1999).

35 CP Blobel, *Nat Rev Mol Cell Biol*, **6**, 32–43 (2005).

36 M Asakura, M Kitakaze, S Takashima, Y Liao, F Ishikura, T Yoshinaka, H Ohmoto, K Node, K Yoshino, H Ishiguro, H Asanuma, S Sanada, Y Matsumura, H Takeda, S Beppu, M Tada, M Hori and S Higashiyama, *Nat Med*, **8**, 35–40 (2002).

37 K Iba, R Albrechtsen, B Gilpin, C Frohlich, F Loechel, A Zolkiewska, K Ishiguro, T Kojima, W Liu, JK Langford, RD Sanderson, C Brakebusch, R Fassler and UM Wewer, *J Cell Biol*, **149**, 1143–56 (2000).

38 A Gaultier, H Cousin, T Darribere and D Alfandari, *J Biol Chem*, **277**, 23336–44 (2002).

39 A Zolkiewska, *Exp Cell Res*, **252**, 423–31 (1999).

40 MJ Duffy, DJ Lynn, AT Lloyd and CM O'Shea, *Thromb Haemost*, **89**, 622–31 (2003).

41 ML Moss and JW Bartsch, *Biochemistry*, **43**, 7227–35 (2004).

42 P Van Eerdewegh, RD Little, J Dupuis, RG Del Mastro, K Falls, J Simon, D Torrey, S Pandit, J McKenny, K Braunschweiger, A Walsh, Z Liu, B Hayward, C Folz, SP Manning, A Bawa, L Saracino, M Thackston, Y Benchekroun, N Capparell, M Wang, R Adair, Y Feng, J Dubois, MG FitzGerald, H Huang, R Gibson, KM Allen, A Pedan, MR Danzig, SP Umland, RW Egan, FM Cuss, S Rorke, JB Clough, JW Holloway, ST Holgate and TP Keith, *Nature*, **418**, 426–30 (2002).

43 D Okuda, H Koike and T Morita, *Biochemistry*, **41**, 14248–54 (2002).

44 LA Hite, JD Shannon, JB Bjarnason and JW Fox, *Biochemistry*, **31**, 6203–11 (1992).

45 H Takeya, S Nishida, N Nishino, Y Makinose, T Omori-Satoh, T Nikai, H Sugihara and S Iwanaga, *J Biochem (Tokyo)*, **113**, 473–83 (1993).

46 TF Huang, JC Holt, H Lukasiewicz and S Niewiarowski, *J Biol Chem*, **262**, 16157–63 (1987).

47 JJ Calvete, C Marcinkiewicz, D Monleon, V Esteve, B Celda, P Juarez and L Sanz, *Toxicon*, **45**, 1063–74 (2005).

48 JP Evans, *Bioessays*, **23**, 628–39 (2001).

49 S Takeda, T Igarashi, H Mori and S Araki, *EMBO J*, **25**, 2388–96 (2006).

50 F Grams, R Huber, LF Kress, L Moroder and W Bode, *FEBS Lett*, **335**, 76–80 (1993).

51 T Igarashi, Y Oishi, S Araki, H Mori and S Takeda, *Acta Crystallogr, Sect F: Struct Biol Cryst Commun*, **62**, 688–91 (2006).

52 FX Gomis-Ruth, LF Kress and W Bode, *EMBO J*, **12**, 4151–57 (1993).

53 FX Gomis-Ruth, LF Kress, J Kellermann, I Mayr, X Lee, R Huber and W Bode, *J Mol Biol*, **239**, 513–44 (1994).

54 D Zhang, I Botos, FX Gomis-Ruth, R Doll, C Blood, FG Njoroge, JW Fox, W Bode and EF Meyer, *Proc Natl Acad Sci USA*, **91**, 8447–51 (1994).

55 W Gong, X Zhu, S Liu, M Teng and L Niu, *J Mol Biol*, **283**, 657–68 (1998).

56 L Watanabe, JD Shannon, RH Valente, A Rucavado, A Alape-Giron, AS Kamiguti, RD Theakston, JW Fox, JM Gutierrez and RK Arni, *Protein Sci*, **12**, 2273–81 (2003).

57 T Kumasaka, M Yamamoto, H Moriyama, N Tanaka, M Sato, Y Katsube, Y Yamakawa, T Omori-Satoh, S Iwanaga and T Ueki, *J Biochem (Tokyo)*, **119**, 49–57 (1996).

58 KF Huang, SH Chiou, TP Ko, JM Yuann and AH Wang, *Acta Crystallogr, Sect D: Biol Crystallogr*, **58**, 1118–28 (2002).

59 X Zhu, M Teng and L Niu, *Acta Crystallogr, Sect D: Biol Crystallogr*, **55**, 1834–41 (1999).

60 Z Lou, J Hou, X Liang, J Chen, P Qiu, Y Liu, M Li, Z Rao and G Yan, *J Struct Biol*, **152**, 195–203 (2005).

61 Y Fujii, D Okuda, Z Fujimoto, K Horii, T Morita and H Mizuno, *J Mol Biol*, **332**, 1115–22 (2003).

62 S Bilgrami, S Tomar, S Yadav, P Kaur, J Kumar, T Jabeen, S Sharma and TP Singh, *J Mol Biol*, **341**, 829–37 (2004).

63 S Bilgrami, S Yadav, P Kaur, S Sharma, M Perbandt, C Betzel and TP Singh, *Biochemistry*, **44**, 11058–66 (2005).

64 M Paz Moreno-Murciano, D Monleon, C Marcinkiewicz, JJ Calvete and B Celda, *J Mol Biol*, **329**, 135–45 (2003).

65 V Saudek, RA Atkinson and JT Pelton, *Biochemistry*, **30**, 7369–72 (1991).

66 H Senn and W Klaus, *J Mol Biol*, **232**, 907–25 (1993).

67 M Adler, RA Lazarus, MS Dennis and G Wagner, *Science*, **253**, 445–48 (1991).

68 J Shin, SY Hong, K Chung, I Kang, Y Jang, DS Kim and W Lee, *Biochemistry*, **42**, 14408–15 (2003).

69 DH Souza, HS Selistre-de-Araujo, AM Moura-da-Silva, MS Della-Casa, G Oliva and RC Garratt, *Acta Crystallogr, Sect D: Biol Crystallogr*, **57**, 1135–37 (2001).

70 J Zang, Z Zhu, Y Yu, M Teng, L Niu, Q Huang, Q Liu and Q Hao, *Acta Crystallogr, Sect D: Biol Crystallogr*, **59**, 2310–12 (2003).

71 K Maskos, C Fernandez-Catalan, R Huber, GP Bourenkov, H Bartunik, GA Ellestad, P Reddy, MF Wolfson, CT Rauch, BJ Castner, R Davis, HR Clarke, M Petersen, JN Fitzner,

DP Cerretti, CJ March, RJ Paxton, RA Black and W Bode, *Proc Natl Acad Sci USA*, **95**, 3408–12 (1998).

72 P Orth, P Reichert, W Wang, WW Prosise, T Yarosh-Tomaine, G Hammond, RN Ingram, L Xiao, UA Mirza, J Zou, C Strickland, SS Taremi, HV Le and V Madison, *J Mol Biol*, **335**, 129–37 (2004).

73 PW Janes, N Saha, WA Barton, MV Kolev, SH Wimmer-Kleikamp, E Nievergall, CP Blobel, JP Himanen, M Lackmann and DB Nikolov, *Cell*, **123**, 291–304 (2005).

74 HS Shieh, KJ Mathis, JM Williams, RL Hills, JF Wiese, TE Benson, JR Kiefer, MH Marino, JN Carroll, JW Leone, AM Malfait, EC Arner, MD Tortorella and A Tomasselli, *J Biol Chem*, **283**, 1501–07 (2007).

75 L Mosyak, K Georgiadis, T Shane, K Svenson, T Hebert, T McDonagh, S Mackie, S Olland, L Lin, X Zhong, R Kriz, EL Reifenberg, LA Collins-Racie, C Corcoran, B Freeman, R Zollner, T Marvell, M Vera, PE Sum, ER Lavallie, M Stahl and W Somers, *Protein Sci*, **17**, 16–21 (2008).

76 Q Zhou, JB Smith and MH Grossman, *Biochem J*, **307**(Pt 2), 411–17 (1995).

77 T Igarashi, S Araki, H Mori and S Takeda, *FEBS Lett*, **581**, 2416–22 (2007).

78 S Takeda, T Igarashi and H Mori, *FEBS Lett*, **581**, 5859–64 (2007).

79 H Takeya, S Nishida, T Miyata, S Kawada, Y Saisaka, T Morita and S Iwanaga, *J Biol Chem*, **267**, 14109–17 (1992).

80 DC Gowda, CM Jackson, P Hensley and EA Davidson, *J Biol Chem*, **269**, 10644–50 (1994).

81 T Morita and GS Bailey (eds.), *Enzymes from Snake Venom*, Alaken, Fort Collins, CO (1998).

82 UM Wewer, M Morgelin, P Holck, J Jacobsen, MC Lydolph, AH Johnsen, M Kveiborg and R Albrechtsen, *J Biol Chem*, **281**, 9418–22 (2006).

83 PJ Kraulis, *Acta Crystallogr, Sect D: Biol Crystallogr*, **24**, 946–50 (1991).

84 EA Merritt and ME Murphy, *Acta Crystallogr*, **D50**, 869–79 (1994).

85 W Bode, FX Gomis-Ruth, R Huber, R Zwilling and W Stocker, *Nature*, **358**, 164–67 (1992).

86 W Bode, P Reinemer, R Huber, T Kleine, S Schnierer and H Tschesche, *EMBO J*, **13**, 1263–69 (1994).

87 WL DeLano, *The PyMOL User's Manual*, DeLano Scientific, San Carlos, CA (2002).

88 T Nikai, K Taniguchi, Y Komori, K Masuda, JW Fox and H Sugihara, *Arch Biochem Biophys*, **378**, 6–15 (2000).

89 JW Fox and JB Bjarnason, *Methods Enzymol*, **248**, 368–87 (1995).

90 KG Mann, *Chest*, **124**, 4S–10S (2003).

91 WI Weis, R Kahn, R Fourme, K Drickamer and WA Hendrickson, *Science*, **254**, 1608–15 (1991).

92 H Mizuno, Z Fujimoto, H Atoda and T Morita, *Proc Natl Acad Sci USA*, **98**, 7230–34 (2001).

93 AS Kamiguti, P Gallagher, C Marcinkiewicz, RD Theakston, M Zuzel and JW Fox, *FEBS Lett*, **549**, 129–34 (2003).

94 Y Usami, Y Fujimura, S Miura, H Shima, E Yoshida, A Yoshioka, K Hirano, M Suzuki and K Titani, *Biochem Biophys Res Commun*, **201**, 331–39 (1994).

95 K Shimokawa, JD Shannon, LG Jia and JW Fox, *Arch Biochem Biophys*, **343**, 35–43 (1997).

96 PB Clissa, M Lopes-Ferreira, MS Della-Casa, SH Farsky and AM Moura-da-Silva, *Toxicon*, **47**, 591–96 (2006).

97 LG Jia, XM Wang, JD Shannon, JB Bjarnason and JW Fox, *Arch Biochem Biophys*, **373**, 281–86 (2000).

98 SM Serrano, LG Jia, D Wang, JD Shannon and JW Fox, *Biochem J*, **391**, 69–76 (2005).

99 SM Serrano, J Kim, D Wang, B Dragulev, JD Shannon, HH Mann, G Veit, R Wagener, M Koch and JW Fox, *J Biol Chem*, **281**, 39746–56 (2006).

100 SM Serrano, D Wang, JD Shannon, AF Pinto, RK Polanowska-Grabowska and JW Fox, *FEBS J*, **274**, 3611–21 (2007).

101 AF Pinto, RM Terra, JA Guimaraes and JW Fox, *Arch Biochem Biophys*, **457**, 41–46 (2007).

102 D Alfandari, H Cousin, A Gaultier, K Smith, JM White, T Darribere and DW DeSimone, *Curr Biol*, **11**, 918–30 (2001).

103 KM Smith, A Gaultier, H Cousin, D Alfandari, JM White and DW DeSimone, *J Cell Biol*, **159**, 893–902 (2002).

104 P Reddy, JL Slack, R Davis, DP Cerretti, CJ Kozlosky, RA Blanton, D Shows, JJ Peschon and RA Black, *J Biol Chem*, **275**, 14608–14 (2000).

Human Molecular Genetics, 2008, Vol. 18, No. ? *1–11*
doi:10.1093/hmg/ddn408
Advance Access published on xxx

Dominant-negative inhibition of Ca^{2+} influx via TRPV2 ameliorates muscular dystrophy in animal models

Yuko Iwata[1,*], Yuki Katanosaka[1], Yuji Arai[2], Munekazu Shigekawa[1,†] and Shigeo Wakabayashi[1]

[1]Department of Molecular Physiology and [2]Department of Bioscience, National Cardiovascular Center Research Institute Suita, Osaka 565-8565, Japan

Received August 19, 2008; Revised and Accepted December 1, 2008

Muscular dystrophy is a severe degenerative disorder of skeletal muscle characterized by progressive muscle weakness. One subgroup of this disease is caused by a defect in the gene encoding one of the components of the dystrophin–glycoprotein complex, resulting in a significant disruption of membrane integrity and/or stability and, consequently, a sustained increase in the cytosolic Ca^{2+} concentration ($[Ca^{2+}]_i$). In the present study, we demonstrate that muscular dystrophy is ameliorated in two animal models, dystrophin-deficient *mdx* mice and δ-sarcoglycan-deficient BIO14.6 hamsters by dominant-negative inhibition of the transient receptor potential cation channel, TRPV2, a principal candidate for Ca^{2+}-entry pathways. When transgenic (Tg) mice expressing a TRPV2 mutant in muscle were crossed with *mdx* mice, the $[Ca^{2+}]_i$ increase in muscle fibers was reduced by dominant-negative inhibition of endogenous TRPV2. Furthermore, histological, biochemical and physiological indices characterizing dystrophic pathology, such as an increased number of central nuclei and fiber size variability/fibrosis/apoptosis, elevated serum creatine kinase levels, and reduced muscle performance, were all ameliorated in the *mdx*/Tg mice. Similar beneficial effects were also observed in the muscles of BIO14.6 hamsters infected with adenovirus carrying mutant TRPV2. We propose that TRPV2 is a principal Ca^{2+}-entry route leading to a sustained $[Ca^{2+}]_i$ increase and muscle degeneration, and that it is a promising therapeutic target for the treatment of muscular dystrophy.

INTRODUCTION

Muscular dystrophy is a heterogeneous genetic disease that causes severe skeletal muscle degeneration characterized by fiber weakness and muscle fibrosis, severe local inflammation and, at least initially, muscle regeneration. A subset of muscular dystrophy is caused by a mutation in the gene encoding one of the components of the dystrophin–glycoprotein complex (DGC) (1–3), a multi-subunit complex (2,4,5) that spans the sarcolemma to structurally link the extracellular matrix and actin cytoskeleton (6). Therefore, disruption of the DGC could significantly disrupt membrane integrity or stability during muscle contraction and relaxation and prevent myocyte survival. The enhanced susceptibility to exercise-induced muscle fiber damage is observed in dystrophic animals, such as δ-sarcoglycan (SG)-deficient BIO14.6 hamsters and dystrophin-deficient *mdx* mice, which are genetic homologues of human limb-girdle and Duchenne muscular dystrophy (DMD), respectively.

Although many studies have molecularly characterized the genes responsible for and the histological pathology of dystrophic tissues, little is known about the pathways by which the genetic defects lead to muscle degeneration. A number of studies have reported the chronic elevation of the cytosolic Ca^{2+} concentration ($[Ca^{2+}]_i$) beneath the sarcolemma or within other cell compartments of skeletal muscle fibers, or in cultured myotubes from dystrophin-deficient DMD patients and *mdx* mice. Increased $[Ca^{2+}]_i$ could activate Ca^{2+}-dependent proteases and promote protein degradation and cell necrosis (7–9). Several pathways leading to an increase of the $[Ca^{2+}]_i$ have been suggested to be involved in the pathology of muscular dystrophy (10–15). We previously identified a stretch-activated channel, the transient receptor potential (TRP) cation channel

*To whom correspondence should be addressed at: Department of Molecular Physiology, National Cardiovascular Center Research Institute, Fujishiro-dai 5-7, Suita, Osaka 565-8565, Japan. Tel: +81 668335012; Fax: +81 668355314; Email: yukoiwat@ri.ncvc.go.jp
†Present address: Department of Human Life Science, Senri Kinran University, Suita, Osaka 565-0873, Japan.

TRPV2, that may function in the pathogenesis of myocyte degeneration caused by DGC disruption (16). The TRP channels form a large family of cation channels that likely function as tetramers in various processes, such as sensory signaling (17–19). The cellular function of TRPV2, however, remains to be characterized. We previously found that TRPV2 normally localizes in the intracellular membrane compartments but translocates to the plasma membrane in dystrophic muscle fibers, thus contributing to a sustained $[Ca^{2+}]_i$ increase (16).

To determine the relationship between TRPV2 activation and muscle degeneration, and determine whether TRPV2 inhibition potentially prevents muscular dystrophy, we introduced mutant TRPV2 into dystrophic muscles to inhibit endogenous TRPV2 activity via a dominant-negative effect. Here we report that transgenic (Tg) or adenoviral expression of dominant-negative TRPV2 ameliorates muscle pathology in *mdx* mice and BIO14.6 hamsters by preventing abnormal Ca^{2+} handling.

RESULTS

Characterization of dominant-negative TRPV2 mutants

Conserved acidic residues in the putative pore region of TRP cation channels are known to be crucial for cation permeation (20,21). We generated three TRPV2 mutants by substituting two highly conserved glutamate residues (Glu594 and Glu604) in the putative pore region with lysine, either individually (E594K and E604K) or together (DK). The TRPV2 mutants were stably expressed in Chinese hamster ovary (CHO) cells, as confirmed by immunoblot, which showed two protein bands with different degrees of glycosylation (Fig. 1B). The immunofluorescence of TRPV2 expressed in CHO cells revealed that, in the absence of serum, most TRPV2 was localized in the intracellular membrane compartments (Fig. 1C). In contrast, upon stimulation with serum, a portion of TRPV2 translocated to the surface membranes (Fig. 1C) as previously reported (22). Interestingly, a similar serum-induced translocation occurred with the three TRPV2 mutants (Fig. 1C, data not shown for E594K and DK).

We next assessed TRPV2 activity by measuring the Ca^{2+}-induced change of the $[Ca^{2+}]_i$ by ratiometric scanning of the fura-2 fluorescence. As shown in Fig. 1D, the perfusion of cells with a 2 mM $CaCl_2$ solution resulted in a rapid and large increase in the $[Ca^{2+}]_i$ of cells expressing wild-type TRPV2 compared to non-transfected control cells (Supplementary Material, Fig. S1). In contrast, the increase in $[Ca^{2+}]_i$ did not occur in cells expressing E604K (Fig. 1D) or the other two mutants (Fig. 1E), suggesting that these mutations abolished Ca^{2+}-permeation via TRPV2. Because the TRP channel family likely functions as tetramers (17,18), we predicted that the TRPV2 mutants would have a dominant-negative effect on wild-type TRPV2 activity. We transiently transfected green fluorescent protein (GFP)-tagged TRPV2 mutants in cells stably expressing wild-type TRPV2 and measured the $[Ca^{2+}]_i$ in GFP-positive cells (Supplementary Material, Fig. S1). Transfection with the mutants dramatically diminished the Ca^{2+}-induced rise (Fig. 1F), suggesting that the TRPV2 mutants exerted a strong dominant-negative effect. Similar inhibitory effects of the mutants were also observed in HEK293 cells when the $[Ca^{2+}]_i$ increase was induced with high Ca^{2+} solution or the TRPV channel agonist 2-aminoethoxydiphenyl borate (2-APB) (Supplementary Material, Fig. S2). Wild-type and mutant TRPV2 were co-localized in the plasma membranes of HEK293 cells (Supplementary Material, Fig. S2). Furthermore, surface biotinylation and co-immunoprecipitation assays revealed that mutant TRPV2 is capable of forming oligomers with wild-type TRPV2 in the cell surface (Supplementary Material, Fig. S3).

Transgenic expression of dominant-negative TRPV2 blocks abnormal Ca^{2+} handling in *mdx* mice

To assess the relationship between TRPV2 activation and muscle degeneration, we analyzed whether the expression of dominant-negative TRPV2 prevents muscle damage in dystrophin-deficient *mdx* mice. We first generated transgenic mice (C57/BL6J background) expressing the hemaglutinin (HA)-tagged E604K (E604K-HA) mutant under the control of the α-skeletal actin promoter in skeletal muscle. Two lines of male Tg mice were then crossed with female *mdx* mice, and because muscular dystrophy is X-linked recessive in *mdx* mice, the resulting male mice were predicted to express the E604K-HA mutant and be deficient in dystrophin. The expression of the E604K-HA mutant was confirmed by anti-HA immunoblotting only in the Tg and *mdx*/Tg mice, although only half level of E604K-HA expression was detected in the latter mice as expected from heterozygotes (Fig. 2A). Interestingly, the level of endogenous TRPV2 was elevated by approximately 2-fold in *mdx* mice compared to controls, but TRPV2 levels were reduced in the *mdx*/Tg mice (Fig. 2A). While endogenous TRPV2 was broadly distributed in the skeletal muscle of control mice (Fig. 2Ba), it almost exclusively localized in the sarcolemma of *mdx* muscles (Fig. 2Bb). On the other hand, exogenous E604K-HA was mostly observed in the intracellular membranes, although a small portion was localized in the sarcolemma (Fig. 2Bg and h). In addition, the expression of E604K-HA reduced the sarcolemmal localization of endogenous TRPV2 in *mdx* muscles (Figs 2Bc and 3Ad, also see Supplementary Material, Fig. S4).

We isolated the Flexor digitorum brevis (FDB) fibers from each mouse and immunostained with the anti-TRPV2 antibody, revealing that, consistent with immunostaining in muscle sections, most TRPV2 localized in the sarcolemma of *mdx* fibers (Fig. 3Ab), but not in the fibers from wild-type mice (Fig. 3Aa); this sarcolemmal localization was much lower in the *mdx*/Tg mice (Fig. 3Ad). Consistent with the sarcolemmal localization of TRPV2 in *mdx* fibers, the perfusion of fibers with 2-APB induced a large and rapid increase in $[Ca^{2+}]_i$ in fibers from *mdx* mice, which was completely inhibited by the TRPV channel antagonist ruthenium red (Fig. 3B). An increase in $[Ca^{2+}]_i$ was also observed to occur upon perfusion with high Ca^{2+} solution (2–5 mM, see Fig. 3B and Supplementary Material, Fig. S5). These Ca^{2+} increases were reduced in fibers from *mdx*/Tg mice (Fig. 3B–D and Supplementary Material, Fig. S5), suggesting that the introduction of E604K-HA inhibited Ca^{2+}-entry via endogenous TRPV2. Since TRPV2 is a stretch-activated channel, we analyzed the effect of mechanical stress on membrane deformation of isolated fibers. We observed that hypo-osmotic stress (70% osmolarity) resulted in severe damage in fibers from *mdx*